Nonequilibrium Green's function study of Pd_4-cluster-functionalized carbon nanotubes as hydrogen sensors

Chao Cao,[1,2] A. F. Kemper,[1,2] Luis Agapito,[1,2] Jian-Wei Zhang,[1,2] Yao He,[1,2] Andrew Rinzler,[1] Hai-Ping Cheng,[1,2,*] X.-G. Zhang,[3] Alexandre Reily Rocha,[4] and Stefano Sanvito[4]

[1]*Department of Physics, University of Florida, Gainesville, Florida 32611, USA*

[2]*Quantum Theory Project, University of Florida, Gainesville, Florida 32611, USA*

[3]*Center for Nanophase Materials Sciences and Computer Science and Mathematics Division, Oak Ridge National Laboratory, Oak Ridge, Tennessee 37831, USA*

[4]*School of Physics, Trinity College, Dublin 2, Ireland*

(Received 25 March 2008; revised manuscript received 12 December 2008; published 27 February 2009)

Pd-cluster-functionalized carbon nanotubes (CNTs) have been shown experimentally to be effective hydrogen sensors. Semiconducting CNTs exhibit much higher sensitivity than ensemble (mixed) ones. Using the nonequilibrium Green's function method combined with the density-functional theory, we simulate and contrast the (8,0) semiconducting and the (5,5) metallic CNT model systems. We find that the electron localization effect plays a crucial role in determining electron transport. Pd clusters and hydrogen adsorption cause opposite effects on electron localization in the CNT backbone for the semiconducting CNT-based systems. Consequently Pd functionalization dramatically increases the conductance, but then it is strongly suppressed by hydrogen absorption. For the metallic CNT-based systems, there is a tiny shift of the transmission peak near the Fermi energy. These results offer a consistent explanation for the experiments.

DOI: 10.1103/PhysRevB.79.075127 PACS number(s): 72.80.Rj, 73.63.Fg, 73.21.Hb

I. INTRODUCTION

Single-walled carbon nanotubes (SWCNTs) are considered to be promising materials and building blocks for future electronic device applications.[1–3] The study of metal–carbon nanotube (CNT) interaction, including metal-CNT contacts, metal-doped, and metal-coated SWCNTs has therefore drawn much attention in the last decades. It has been demonstrated that CNTs can be used as chemical sensors that are capable of detecting small concentrations of molecules with high sensitivity under ambient conditions.[4–14] Thus CNT-based sensors have potential impact on a wide range of human activities, from domestic gas alarms, space missions, agricultural and medical diagnostic apparatuses, to chemical plant instruments for safety control.[15] Traditional gas sensors, such as semiconductor metal oxides, silicon, organic materials, and carbon black polymer composites, are known to be only operable at high temperatures (200–600 °C) due to the chemical reaction barrier between the sensing materials and the gas molecules. Hole-doped semiconductor CNTs, however, have been proven to have substantial conductance change upon exposure to NO_2 and NH_3 molecules at room temperature,[5] and thus shed light on room-temperature electrical sensing.

Among all CNT-based sensors, palladium-doped CNTs have drawn special attention. Recently, experiments demonstrated that Pd-doped or Pd-coated CNTs can be used as a hydrogen sensor.[6–14,16] In these experiments, ensemble (mixed) SWCNTs show a limited hydrogen sensitivity, while semiconducting SWCNTs show a nearly 50% conductance change in the presence of hydrogen. Experimentalists were also able to identify that the palladium forms noncontinuous, closely deposited clusterlike structures.[6,8] Theoretically, Miao *et al.*[17] employed a continuous atomic chain model and studied band structure of Pd and Pd/Ni alloy chain-doped CNT using density-functional theory (DFT). Their results showed that hydrogen adsorption modifies the density of states (DOS) around E_F dramatically in both semiconducting and metallic CNTs, and therefore causes the conductance change observed experimentally. In our previous work,[18] we studied the band structure of Pd_4-cluster-functionalized (5,5) CNTs, and concluded that the hydrogen adsorption reduces the electron localization effect. Hence the conductance of Pd_4-cluster-functionalized metallic CNTs is expected to increase upon hydrogen adsorption. Nevertheless, no transport calculation is available at the moment, and it is still not clear what the sensing mechanism is or why there is such a large difference between semiconducting and metallic SWCNTs.

In this paper, we report a first-principles investigation of the conductance response of Pd_4-functionalized SWCNTs to hydrogen environment. We examine and contrast semiconducting and metallic SWCNT systems, and reveal the physics behind Pd-doped SWCNT hydrogen sensing. The rest of the paper is organized as follows: in Sec. II, we briefly present our theoretical method and calculation details. Then we present our results of semiconducting (8,0) SWCNTs in parallel with metallic (5,5) SWCNTs, combined with discussion. Finally we summarize the paper and draw conclusions.

II. METHOD AND CALCULATION DETAILS

We combine DFT (Ref. 19) and nonequilibrium Green's function[20,21] (NEGF) method to calculate the electronic structure and transport properties. In particular, we use the SMEAGOL code,[22,23] which implements the NEGF formalism for the single-particle Hamiltonian that is obtained from DFT calculations based on the SIESTA code.[24] It follows the standard three-part division of a transport system, i.e., the left lead, the right lead, and the device region in between the leads. Density-functional theory is used to relax the structure and to construct the Hamiltonian matrices

$$H_{IJ}^{\alpha\beta} = \langle \psi_I^\alpha | H[n] | \psi_J^\beta \rangle \quad (1)$$

and the overlapping matrices

$$S_{IJ}^{\alpha\beta} = \langle \psi_I^\alpha | \psi_J^\beta \rangle,$$

where I and J can be L, R, and D, representing the left lead, the right lead, and the device region, respectively. α and β represent orbital indices; n is the density matrix. This information is then used to calculate the self-energies

$$\Sigma_I^R(E) = (\epsilon^\dagger S_{DI} - H_{DI}) G_{II}^R(E) (\epsilon^\dagger S_{ID} - H_{ID}),$$

where I is either L or R (left or right lead), $\epsilon^\dagger = E + i\eta$, G_{II}^R is the retarded surface Green's function for lead I, and η is an infinitesimal number in order to keep causality. The effective Green's function for the device region can be then calculated as

$$G_D^R(E) = [\epsilon^\dagger S_{DD} - H_{DD} - \Sigma_L^R(E) - \Sigma_R^R(E)]^{-1}. \quad (2)$$

The nonequilibrium Green's function $G^<$ is then

$$G^< = G^R \Sigma^< G^A, \quad (3)$$

where $\Sigma^< = \Sigma_L^< + \Sigma_R^<$ is the sum of the self-energy terms from both leads; $\Sigma_I^<(E) = f_I(E)\Gamma_I$; $f(E)$ is the Fermi distribution function; $i\Gamma_I = \Sigma_I^A - \Sigma_I^R$ is the coupling strength between lead I and device region; and $I = L, R$.

Furthermore, the density matrix and $G^<$ have following relation:

$$n = \frac{i}{2\pi} \int G^<(E) dE. \quad (4)$$

Equations (1)–(4) form a self-consistent set, which can be solved iteratively. After achieving the self-consistency, the transmission coefficient T can be evaluated as

$$T = \frac{2e^2}{h} Tr[\Gamma_L G_D^R \Gamma_R G_D^A].$$

We chose a (5,5) SWCNT as the metallic model system and a (8,0) SWCNT as the semiconducting model system. The transport is along axis of the CNT (z axis), and a large intercell distance was introduced in the x and y directions to eliminate the interactions between two neighboring images. Two tetrahedral Pd_4 clusters were deposited on top of the CNT to form the scattering or reaction center. The leads were chosen to be Au wire in (111) direction, and the lead-molecule distance was optimized to ensure stability. However, the CNT structure and Au surface structure at the interface were kept rigid respectively during the optimization. We argue that the important physics occur at the device region, and the interface introduces nothing but a fixed interface resistance. Therefore, the detailed interface structure is not important to our result. Structures other than the device/lead interface were fully relaxed until the force on each atom was smaller than 0.01 eV/Å. We used the double-zeta split-valence numerical basis sets[25] and the minimal basis sets for the structural optimization and the transport calculations, respectively. Minimal basis sets were used for transport calculations because only the states around E_F are crucial to transport properties. Thus minimal basis set is good enough for this purpose. Also, redundant basis will lead to singular matrix problem when calculating the Green's function. In all calculations, the local-density approximation (LDA) in Perdew-Zunger form[26] was incorporated to describe the exchange correlations of the system, and the electron-density matrix is regarded as converged if $|n_{IJ}^{\text{in}} - n_{IJ}^{\text{out}}| < 1.0 \times 10^{-5}$ in the last self-consistent field (SCF) iteration. The equivalent plane-wave energy cutoff for the real-space grid was taken to be 200 Ry. For the leads, we used a $1 \times 1 \times 32$ Monkhorst scheme k grid[27] to sample the Brillouin zone, while for the device region we take only the gamma point into consideration. In the retarded and advanced Green's function calculations, we set the infinitesimal number $\eta = 1.0 \times 10^{-5}$ to ensure the causality. Finally, we enforce the charge neutrality to be $0.001e$ by matching the Hartree potentials at leads/device region interface.

III. RESULTS AND DISCUSSION

A. Structure

Figures 1 and 2 show the optimized geometries for the device regions of the semiconducting and metallic CNTs, respectively. Even though hydrogen molecules can be either physisorbed or chemisorbed on Pd clusters, the physisorption is rarely observed experimentally due to the small barrier between the two states.[28,29] We simulate both states for completeness and comparison purposes. The Pd_4 clusters form a distorted (slightly elongated along the z axis) tetrahedron on the CNTs due to strong interactions between the carbon and palladium atoms. The Pd-H bond lengths in the physisorbed and chemisorbed complexes are approximately 1.67 and 1.80 Å, respectively. The H-H distance is increased from 0.75 Å (in a H_2 molecule) to 1.00 Å in physisorption, and is further increased to 2.38 Å in chemisorption.

B. Electronic structure analysis

1. Transmission coefficient

We show the NEGF calculation of the conductance in Fig. 3. The small bias conductance near E_F corresponds to the quantity measured in most experiments. The conductances of pure (5,5) and (8,0) CNTs without Pd doping are $0.62G_0$ and $0.23G_0$, respectively, where $G_0 = 2e^2/h$ denotes the conductance quanta [Fig. 3(a)]. Note that in Fig. 3(a) there is a finite conductance at E_F for the semiconducting CNT due to the tunneling current. The changes in the conductance after Pd doping and hydrogen absorption are very different for the semiconducting and the metallic CNTs. After Pd doping, the conductance of the metallic CNTs decreases to $0.28G_0$ [Fig. 3(b)], and that of the semiconducting CNTs increases to $0.54G_0$ [Fig. 3(c)].

With the adsorption of hydrogen, the conductance changes are reversed. For the semiconducting CNT-based systems, the conductance is reduced to $0.27G_0$ for physisorption and $0.24G_0$ for chemisorption [Fig. 3(c)]. For the metallic system, hydrogen adsorption enhances the conductance to $0.36G_0$ for physisorption and $0.53G_0$ for chemisorption [Fig. 3(b)].

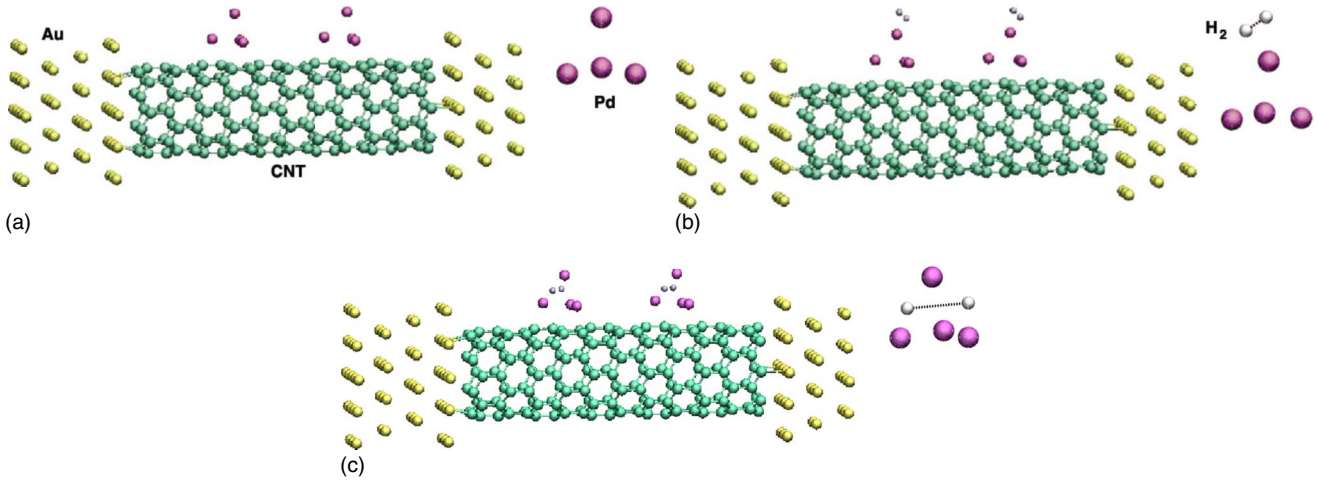

FIG. 1. (Color online) Geometric structures of the semiconducting (8,0) CNT-based systems (a) doped only with palladium, (b) with hydrogen molecule physisorbed on palladium, and (c) with hydrogen molecule chemisorbed on palladium. Yellow atoms are Au in leads; green atoms are carbon; magenta atoms are palladium; and white atoms are hydrogen. The top right inset of each panel shows the local structure of Pd cluster from front view. The dotted line shows the H-H bond.

To compare with experimental results, we define the sensitivity as

$$\text{sensitivity} = \max\left[\frac{G_f}{G_i}, \frac{G_i}{G_f}\right], \tag{5}$$

where G_f is the palladium-doped system conductance after hydrogen adsorption, and G_i is the palladium-doped system conductance before hydrogen adsorption. From the conductances calculated above, a pure (8,0) semiconducting sensing system has a sensitivity of ~2. For a mixed ensemble system consisting of 1/3 metallic CNTs and 2/3 semiconducting CNTs, if we assume that all CNTs are in a parallel configuration and use the conductance calculated for both systems, our model system gives a sensitivity of ~1.35 because the metallic system conductance varies in the opposite direction from the semiconducting systems. If as we argued that the conductance of the metallic systems varies much less than the zero-bias conductance calculated at E_F, then the sensitivity of the mixed ensemble is increased slightly above 1.49 but still significantly below 2. These results perfectly match the experiments performed by Kong *et al.*,[6] which measured sensitivities of ~2 and ~1.36, respectively, for the semiconductor-based systems and the mixed ensemble systems. The conductance increase in the metallic CNT-based systems is also consistent with our previous band-structure calculation of (5,5) CNT-based systems.[18]

2. Density of states

To analyze the physics behind different behavior induced by Pd_4-cluster doping, we first calculated the electronic DOS

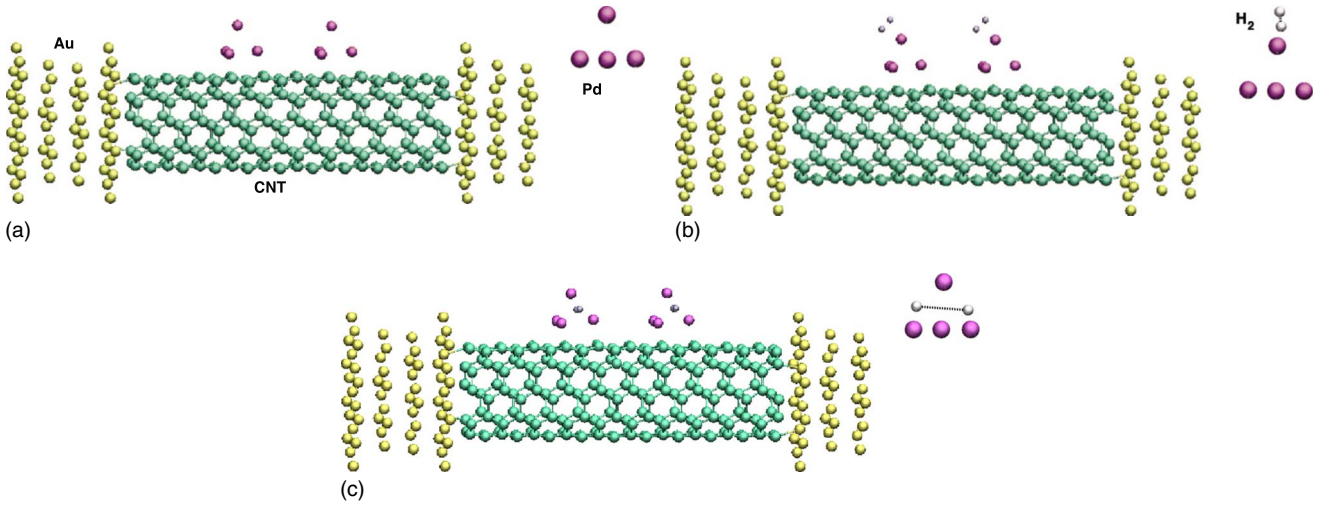

FIG. 2. (Color online) Geometric structures of the metallic (5,5) CNT-based systems (a) doped only with palladium, (b) with hydrogen molecule physisorbed on palladium, and (c) with hydrogen molecule chemisorbed on palladium. Yellow atoms are Au in leads; green atoms are carbon; magenta atoms are palladium; and white atoms are hydrogen. The top right inset of each panel shows the local structure of Pd cluster from front view. The dotted line shows the H-H bond.

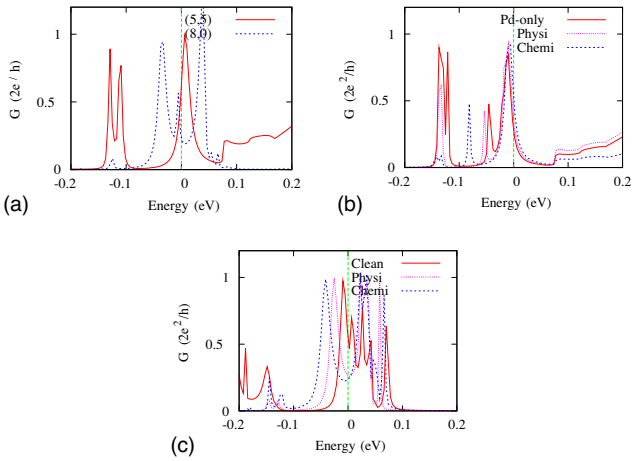

FIG. 3. (Color online) Transmission spectra of (a) pure CNTs within gold leads (without any Pd or hydrogen doping), (b) metallic (5,5) CNT-based systems, and (c) semiconducting (8,0) CNT-based systems. "Pd only" indicates Pd-cluster-doped CNT system without hydrogen adsorption; "Physi" indicates hydrogen-physisorbed system; and "Chemi" indicates hydrogen-chemisorbed system. E_F is aligned at 0.0 eV in all figures.

and projected DOS onto the CNT backbone for both metallic and semiconducting systems without hydrogen adsorption as shown in Figs. 4(a) and 4(b). For the metallic CNTs [Fig. 4(a)], the result confirms that obtained in a previous work.[18] Bonding with the Pd cluster causes the localized states to form at CNT/Pd-cluster interface. This should add considerable scattering to the conduction channels, and as we will show below should significantly reduce the conductance. For the semiconducting CNTs, the projected DOS of pure CNT and CNT with Pd doping [Fig. 4(b)] shows that the presence of Pd cluster greatly reduces the band gap, from ~0.8 to ~0.4 eV. This is expected to significantly increase the conductance.

Realistic CNT-based systems are usually much longer than our model systems, but simulating systems with a much longer length is not computationally feasible. Therefore, in order to see possible effects of Pd doping and hydrogen adsorption on longer CNTs, we present the projected DOS calculation of model systems without the gold leads (Fig. 5). By eliminating the gold leads, we can focus on the change within scattering center area that more closely mimics the part of the CNTs far away from the electrodes in a realistic system. The metallic CNT-based system shows a similar reduced electron localization effect with hydrogen chemisorption since the state around E_F in the top panel is much more extended than in the bottom panel. The semiconducting CNT-based system exhibits an even larger localization effect that the band gap at E_F is again enlarged.

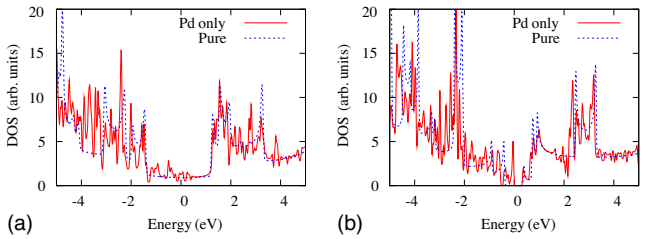

FIG. 4. (Color online) DOSs around E_F projected onto CNT backbone for the pure and Pd-cluster-doped CNT systems without gold leads. E_F is aligned at 0. Panel (a): metallic (5,5)-based systems; panel (b): semiconducting (8,0)-based systems.

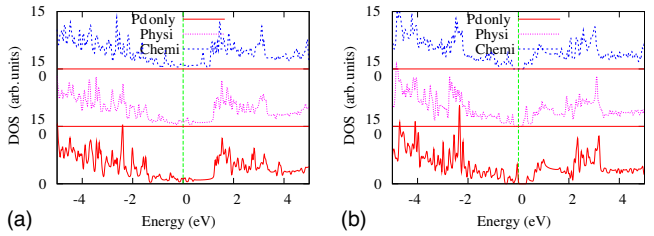

FIG. 5. (Color online) DOSs of model systems without gold leads projected onto CNT backbone: (a) metallic (5,5) CNT-based systems; (b) semiconducting (8,0) CNT-based systems. E_F is aligned at 0.

3. Charge transfer and Hartree potential

To further understand the sensing mechanism, we performed the Mülliken population analysis (Table I) on our model systems. For pure CNTs, the Pd doping causes ~5.6e and ~4.6e transferred to the metallic and the semiconducting systems from the Pd clusters, respectively. These charge transfers cause different effects in the two types of systems. For the semiconducting system, the charge transfer causes a significant shift in the conductance peaks and brings one of the peaks very close to E_F, thus leading to a large increase in the conductance. For the metallic system, however, the shift in the conductance peak near E_F is much smaller, less than 0.01 eV. The large change in the conductance is mainly due to the sharpness of the peak. When integrated over a typical bias voltage window, the effect of the charge transfer on the conductance in the metallic system should be greatly reduced.

For hydrogen-adsorbed systems, the charge analysis shows that both hydrogen physisorption and chemisorption will further deplete charge on Pd clusters by ~0.1e. Interestingly, no significant difference between physisorption and chemisorption is observed on Pd cluster or CNT backbone. However, since the hydrogen atom has much higher electron affinity than Pd cluster after hydrogen dissociation, approxi-

TABLE I. Excess charges in device region and on each atomic species (number of electrons). "Pd only" denotes the Pd-functionalized CNT without hydrogen adsorption; "Physi" denotes hydrogen-physisorbed system; and "Chemi" denotes hydrogen-chemisorbed system.

	(5,5)			(8,0)		
	Pd only	Physi	Chemi	Pd only	Physi	Chemi
C	9.85	9.72	9.65	8.92	8.88	8.79
Pd	−5.65	−5.78	−5.78	−4.63	−4.76	−4.74
Au	−4.20	−4.66	−6.21	−4.29	−4.92	−6.37
H	NA	0.72	2.34	NA	0.80	2.32

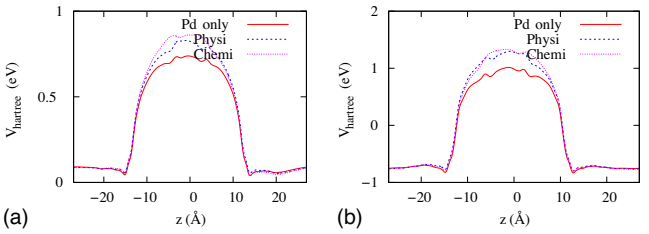

FIG. 6. (Color online) Hartree potentials averaged over the xy cross section of the device region along the z axis for (a) (5,5)-based model systems and (b) (8,0)-based model systems. The two panels should not be compared directly against each other. The curves within each panel, however, are directly comparable. The labels "Pd only," "Physi," and "Chemi" have the same meanings as in Fig. 3.

mately 1.6 more electrons will be transferred onto hydrogen to form Pd-H chemical bonding in chemisorption than in physisorption. A similar amount of electrons was then transferred from Au leads via CNT backbone onto Pd cluster to neutralize the clusters.

The large effect of hydrogen adsorption in the semiconducting systems is again due to the significant shift in the transmission peak relative to E_F, this time in the opposite direction from the case of Pd doping. For the metallic systems, there is still very little shift in the transmission peak. The large changes in the conductance are again due to the tiny shift of a very sharp peak, and are expected to diminish once integrated over a small bias window.

One way to visualize the effect of charge transfers is through the plot of the Hartree potential within the device region, as shown in Fig. 6. Both plots indicate that either hydrogen physisorption or chemisorption substantially modifies the electrostatic potential within the device region. Yet, no big differences are seen at the Au-lead/CNT interfaces (around ± 12 Å). This further supports our initial assumption that the details of the interface are not important factors in understanding the effect of hydrogen adsorption.

4. Local density of states

We now analyze how the local density of states (LDOS) (Figs. 7 and 8) responds to hydrogen adsorption. The LDOS is obtained by integrating the real-space Green's function for the device region:

$$\rho(\mathbf{r}) = -\frac{1}{\pi}\int_{E_F-\delta}^{E_F+\delta} \mathrm{Im}[G(\mathbf{r},\mathbf{r},E)]dE, \tag{6}$$

where we choose $\delta = 0.05$ eV. The figures clearly show that the hydrogen adsorption induced electron localization on CNT backbone for semiconducting CNT systems, which reduces the conductivity approximately by half (Fig. 8). For metallic CNT-based systems, little difference is observed on CNT backbone. However the states at the CNT/Pd-cluster interface are greatly reduced by hydrogen chemisorption. These states are actually strong chemical bonding between CNT and Pd cluster,[18] which serves as a scattering center in device region. Thus, the hydrogen chemisorption enhances the electron transport.

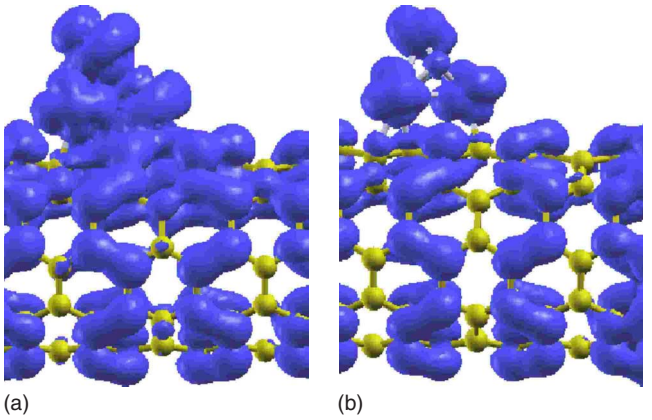

FIG. 7. (Color online) LDOSs of metallic (5,5) CNT-based systems. The contour is taken at LDOS of 1.0×10^{-4}. The figure shows only one of the two CNT-cluster units for simplicity and clearness purposes. (a) Pd-cluster-doped CNT without hydrogen adsorption; (b) Pd-cluster-doped CNT with hydrogen chemisorption.

C. Length dependence and interference effects

Finally, we use two more systems to investigate the length dependence and possible interference between two Pd_4 clusters. For one of these systems, we remove one of the functioning Pd_4 clusters together with the underlying CNT, and therefore the effective length of the device region is reduced by half. We will refer to this system as "reference system A." For the other system, we add one more unit cell of pure CNT in between the two Pd clusters, so that the distance between the two Pd clusters is increased. We will refer to this system as "reference system B." Both structures are relaxed with the same procedure and criterion as previously stated.

Figures 9(a) and 9(b) show the transmission coefficient spectrum of reference system A. Apparently, they are very different from Figs. 3(b) and 3(c). Although we can still identify the corresponding peaks in Figs. 9(a) and 9(b), their heights and widths are completely different from those in

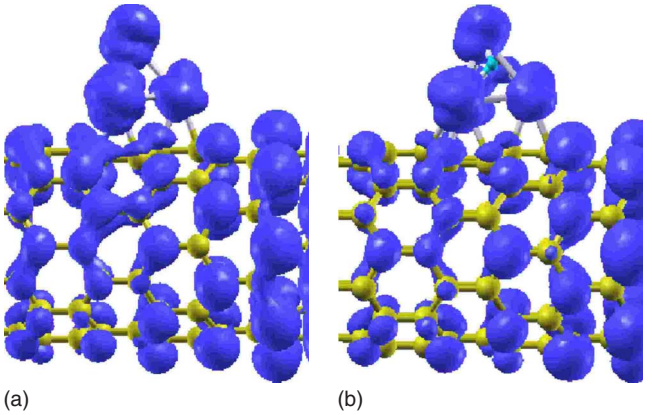

FIG. 8. (Color online) LDOSs of semiconducting (8,0) CNT-based systems. The contour is taken at LDOS of 1.0×10^{-4}. The figure shows only one of the two CNT-cluster units for simplicity and clearness purposes. (a) Pd-cluster-doped CNT without hydrogen adsorption; (b) Pd-cluster-doped CNT with hydrogen chemisorption.

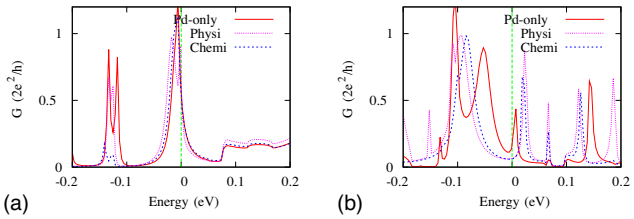

FIG. 9. (Color online) Transmission spectra of reference system A for (a) (5,5) metallic CNT-based systems and (b) (8,0) semiconducting CNT-based systems. "Pd-only" denotes the system without hydrogen adsorption; "Physi" denotes the system with hydrogen physisorbed on the cluster; and "Chemi" denotes the system with hydrogen chemisorbed on the cluster.

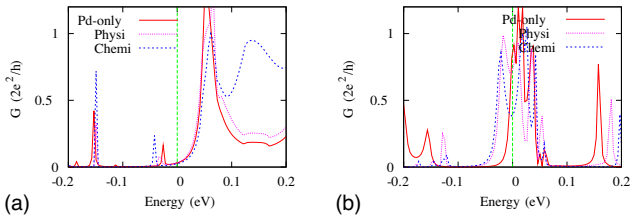

FIG. 10. (Color online) Transmission spectra of reference system B for (a) (5,5) metallic CNT-based systems and (b) (8,0) semiconducting CNT-based systems. "Pd-only" denotes the system without hydrogen adsorption; "Physi" denotes the system with hydrogen physisorbed on the cluster; and "Chemi" denotes the system with hydrogen chemisorbed on the cluster.

Figs. 3(b) and 3(a). Nevertheless, the conductances of metallic CNT-based systems without hydrogen adsorption, with hydrogen physisorption, and with hydrogen chemisorption are $0.567G_0$, $0.645G_0$, and $0.541G_0$, respectively, showing almost no sensitivity ($\sim$1). The conductances of semiconducting CNT-based systems without hydrogen adsorption, with hydrogen physisorption, and with hydrogen chemisorption are $0.209G_0$, $0.067G_0$, and $0.063G_0$, respectively. This corresponds to sensitivity of $\sim$3. Although the specific conductance number changes a lot, the relative conductance change after hydrogen adsorption is rather stable. Thus our fundamental conclusion remains unchanged.

The influence of interference can also be observed in Figs. 10(a) and 10(b), which show the transmission coefficient spectrum of reference system B. In the (5,5) CNT case, the extra CNT unit causes large shift of the conductance peaks both with and without hydrogen adsorption. The resulting conductances are $0.031G_0$, $0.033G_0$, and $0.025G_0$ for CNT without hydrogen adsorption, CNT with hydrogen physisorption, and CNT with hydrogen chemisorption, respectively. In the (8,0) CNT case, the extra CNT unit also causes shift of the conductance peaks, but the shift does not change the relative positions of these peaks. Therefore, the conductances are $0.87G_0$, $0.74G_0$, and $0.40G_0$ for CNT without hydrogen adsorption, CNT with hydrogen physisorption, and CNT with hydrogen chemisorption, respectively. Thus, the sensitivities for metallic and semiconducting CNTs are $\sim$1 and $\sim$2 in the second comparison systems, respectively. Again, although the specific conductance number changes a lot, the relative conductance changes, and hence the conclusion remains unaltered.

IV. SUMMARY AND CONCLUSION

In conclusion, we have performed DFT-combined NEGF calculations on Pd_4-cluster-functionalized (5,5) and (8,0) CNT model systems. Upon Pd doping, the conductance of metallic CNTs decreases due to electron localization effects, and the conductance of the semiconducting CNTs increases since it creates new states that reduces the band gap. For metallic (5,5) system, the conductance increases by $\sim$90% with hydrogen chemisorption, while for semiconducting (8,0) system, the adsorption suppresses the conductance by $\sim$60%. This behavior is dominated by electron localization effect upon hydrogen adsorption, and is related to charge transfer. Therefore both metallic and semiconducting CNTs are much better hydrogen-sensing materials individually than mixed ensemble CNTs. Although we are unable to mimic a very long CNT/Pd complex system such as those in the experiments, we conclude from this study that the sensitivity of the system is insensitive to the length of the CNT/Pd complex and the displacement of the Pd clusters, meaning that the sensing mechanism is robust.

ACKNOWLEDGMENTS

This work was supported by DOE under Grant No. FG02-02ER45995. The authors want to thank DOE/NERSC, CNMS/ORNL, and the University of Florida High Performance Computing Center for providing computational resources and support that contributed to the research results reported in this paper. Part of this research was also facilitated by the CNMS user program at ORNL from the Division of Scientific User Facilities, U.S. DOE.

*Corresponding author; cheng@qtp.ufl.edu

[1] S. J. Tans, M. H. Devoret, H. Dai, A. Thess, R. E. Smalley, L. J. Geerligs, and C. Dekker, Nature (London) **386**, 474 (1997).
[2] R. H. Baughman, A. A. Zakhidov, and W. A. de Heer, Science **297**, 787 (2002).
[3] S. J. Tans, A. R. M. Verschueren, and C. Dekker, Nature (London) **393**, 49 (1998).
[4] P. G. Collins, K. Bradley, M. Ishigami, and A. Zettle, Science **287**, 1801 (2000).
[5] J. Kong, N. R. Franklin, C. W. Zhou, M. G. Chapline, S. Peng, K. J. Cho, and H. J. Dai, Science **287**, 622 (2000).
[6] J. Kong, M. G. Chapline, and H. J. Dai, Adv. Mater. (Weinheim, Ger.) **13**, 1384 (2001).
[7] J. Sippel-Oakley, H. T. Wang, B. S. Kang, Z. C. Wu, F. Ren, A. G. Rinzler, and S. J. Pearton, Nanotechnology **16**, 2218 (2005).
[8] M. Krishna Kumar and S. Ramaprabhu, Int. J. Hydrogen Energy

32, 2518 (2007).
[9] I. Sayago, E. Terrado, E. Lafuente, M. C. Horrillo, W. K. Maser, A. M. Benito, R. Navarro, E. P. Urriolabeitia, M. T. Martinez, and J. Gutierrez, Synth. Met. **148**, 15 (2005).
[10] U. Schlecht, K. Balasubramanian, M. Burghard, and K. Kern, Appl. Surf. Sci. **253**, 8394 (2007).
[11] J. Suehiro, S.-I. Hidaka, S. Yamane, and K. Imasaka, Sens. Actuators B **127**, 505 (2007).
[12] Y. Sun and H. H. Wang, Adv. Mater. (Weinheim, Ger.) **19**, 2818 (2007).
[13] Y. Sun, H. H. Wang, and M. Xia, J. Phys. Chem. C **112**, 1250 (2008).
[14] M. K. Kumar, A. L. M. Reddy, and S. Ramaprabhu, Sens. Actuators B **130**, 653 (2008).
[15] MRS Bull. **24** (1999), special issue on Gas sensing materials, edited by Joseph Watson.
[16] Y. Li, H. Wang, Y. Chen, and M. Yang, Sens. Actuators B **132**, 155 (2008).
[17] L. Miao, V. R. Bhethanabotla, M. M. Ossowski, and B. Joseph, J. Phys. Chem. B **110**, 22415 (2006).
[18] C. Cao, Y. He, and H.-P. Cheng, Phys. Rev. B **77**, 045412 (2008).
[19] W. Kohn and L. Sham, Phys. Rev. **140**, A1133 (1965).
[20] L. P. Kadanoff and G. Baym, *Quantum Statistical Mechanics* (Benjamin/Cummings, New York, 1962).
[21] S. Dutta, *Electronic Transport in Mesoscopic System* (Cambridge University Press, Cambridge, England, 1995).
[22] A. R. Rocha, V. M. Garcia-Suarez, S. Bailey, C. J. Lambert, J. Ferrer, and S. Sanvito, Nature Mater. **4**, 335 (2005).
[23] A. R. Rocha, V. M. Garcia-Suarez, S. W. Bailey, C. J. Lambert, J. Ferrer, and S. Sanvito, Phys. Rev. B **73**, 085414 (2006).
[24] J. M. Soler, E. Artacho, J. D. Gale, A. Garcia, J. Junquera, P. Ordejon, and D. Sanchez-Portal, J. Phys.: Condens. Matter **14**, 2745 (2002).
[25] J. Junquera, O. Paz, D. Sanchez-Portal, and E. Artacho, Phys. Rev. B **64**, 235111 (2001).
[26] J. P. Perdew, Phys. Rev. B **33**, 8822 (1986).
[27] H. J. Monkhorst and J. D. Pack, Phys. Rev. B **13**, 5188 (1976).
[28] P. K. Schmidt, K. Christmann, G. Kresse, J. Hafner, M. Lischka, and A. Gross, Phys. Rev. Lett. **87**, 096103 (2001).
[29] U. Muschiol, P. K. Schmidt, and K. Christmann, Surf. Sci. **395**, 182 (1998).